Atomic motion in a magneto-optical field

U. Janicke and M. Wilkens
Fakultät für Physik, Universität Konstanz, 78434 Konstanz, Germany
(Received 29 March 1994)

We study the motion of three-level atoms in a magneto-optical field which consists of a laser field with a polarization gradient and a static magnetic field. The Hamiltonian of the model is diagonalized using band-theoretical methods of solid-state theory. Diffraction of atoms is studied numerically, and the results are compared to the ordinary Kapitza-Dirac effect. Spontaneous emission is accounted for by the use of quantum Monte Carlo techniques.

PACS number(s): 42.50.Vk, 32.80.−t

I. INTRODUCTION

Following its first demonstration in the 1980s [1,2], the diffraction of an atomic beam from a standing-wave laser field, the near resonant Kapitza-Dirac effect, has found widespread interest both in applied and fundamental fields of research. In atom optics, coherent beam splitters for atom waves have been demonstrated [3,4] that are based on the diffractive properties of the periodic intensity variations of a standing light field. In atom lithography, the focusing capabilities of the nodes of a standing-wave laser field have been used to write periodic arrays of Cr atoms on a substrate [5]. Beside the transmission of atoms, the quantized atomic motion in the "lattice" of the periodic intensity variations of a standing-wave light field has attracted considerable interest both experimentally [6–9] and theoretically [10–14]. Also, interesting detection schemes have been proposed that are based on the entanglement of the quantized light field and the motion of the atom, opening the possibility to measure the position of an atom [15,16], its momentum [17], or even the photon statistics of the light field [18,19].

In the most common configuration of the near resonant Kapitza-Dirac effect, two-level atoms are considered that move in the one-dimensional "lattice" provided by the *intensity* modulations of a near resonant, *uniformly polarized* standing-wave laser field. Recently, a variation of that classic configuration was conceived by Grimm and co-workers [20–22], where three-level atoms are employed rather than two-level atoms, and the lattice consists of a combination of a laser field with a *polarization gradient* and a static magnetic field aligned parallel with the optical axis of the laser field. Diffraction of atoms in this configuration was analyzed by Pfau and co-workers [23,24] using a combination of the Raman-Nath approximation and the adiabatic approximation. It was found that for short interaction times, the magneto-optical configuration (MOC) could be very efficient in splitting atomic beams, enlarging the achievable splitting angles by orders of magnitude as compared to the performance of the ordinary standing-wave configuration.

This prediction was confirmed in a subsequent experiment by Pfau *et al.* [25], where a supersonic beam of metastable He atoms was split into two outgoing beams differing in transverse momentum by an amount of $\Delta P = 42\hbar k$. The comparably large momentum transfer makes the MOC a very promising candidate for the use as a beam splitter in atom interferometry.

In this paper we present a thorough theoretical study of the magneto-optical configuration, paying particular attention to the effects of finite interaction times and transverse profile of the diffracting laser field. In the language of atom optics, our investigations neither invoke the celebrated Raman-Nath short-time approximation nor the commonly employed adiabatic approximation. These approximation schemes are not used here because experimental capabilities allow for interaction times which go far beyond the Raman-Nath regime, and the resonant beam-splitting observed in [25] involves degeneracies of the quasipotentials where nonadiabatic transitions may occur. The present investigations are based on an exact diagonalization of the Hamiltonian of the magneto-optical configuration, including the kinetic-energy operator of the atoms. The diagonalization is achieved within a band-theoretical framework akin to the one used for the analysis of standing-wave diffraction in [10].

Since we allow for arbitrary interaction times, we also include spontaneous emission, using the method of quantum Monte Carlo simulations recently developed by Carmichael [26] and, independently, by Dalibard and Castin [27]. The treatments used in this paper have already been applied to the usual standing-wave diffraction in the presence of spontaneous emission by Mølmer *et al.* [28].

The paper is organized as follows. In Sec. II we present the model and its band-theoretic formulation. In Sec. III we present results of our simulations. We give an estimate for the relevant time scales and develop a simple classical model which helps one to understand the basic principle of the diffraction of atoms in an arbitrary light field. Finally, Sec. IV contains our conclusions and an outlook on the future prospects of the magneto-optical diffraction scheme.

II. MODEL

A. Hamiltonian

The principal setup of a magneto-optical diffraction experiment is depicted in Fig. 1. An atomic beam travel-

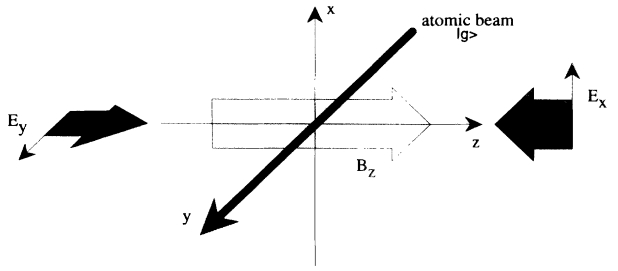

FIG. 1. The principal setup for the magneto-optical interaction.

ing predominantly in the y direction traverses a standing-wave laser field $\mathbf{E}(Z,t)$ with optical axis in the z direction and a homogeneous static magnetic field $\mathbf{B} = B_0\boldsymbol{\epsilon}_z$ which is aligned parallel with the optical axis. Here $\boldsymbol{\epsilon}_z$ is the unit vector in the z direction. The atom is modeled as a symmetric three-level system that consists of a ground state $|g\rangle$ of energy E_g and magnetic quantum number $m = 0$, and a Zeeman doublet of excited states $|e_+\rangle$, $|e_-\rangle$ of energy E_e and magnetic quantum numbers $m = \pm 1$. Without loss of generality, we set $E_g = 0$ and denote as $\omega_{eg} \equiv (E_e - E_g)/\hbar$ the Bohr transition frequency.

Assuming that the atoms are sufficiently fast, we treat their longitudinal motion in the y direction classically and restrict our considerations to the quantum mechanical motion in the z direction. We are thus led to consider the following Hamiltonian:

$$H = \frac{\hat{P}^2}{2M} + H_{\rm at} - \hat{m}_z B_0 - \hat{\mathbf{d}} \cdot \mathbf{E}(\hat{Z},t) \; . \tag{1}$$

Here, $\hat{Z}$ and $\hat{P}$ denote canonically conjugate center-of-mass position and momentum operators for the atomic motion in the z direction. They obey the commutation relation $[\hat{Z},\hat{P}] = i\hbar$. Furthermore, $H_{\rm at} = \hbar\omega_{eg}\left(|e_+\rangle\langle e_+| + |e_-\rangle\langle e_-|\right)$ denotes the Hamiltonian of the free atom, $\hat{m}_z$ is the z component of the magnetic dipole operator, and $\hat{\mathbf{d}}$ denotes the electric dipole transition operator. Expressed in terms of the electronic states we have

$$\hat{m}_z \equiv -\hbar g_J \mu_B \Big(|e_+\rangle\langle e_+| - |e_-\rangle\langle e_-| \Big) \; , \tag{2}$$

where μ_B is the Bohr magneton and g_J is the g factor of the excited states. Decomposing the electric dipole transition operator into its positive and negative frequency parts,

$$\mathbf{d} = \mathbf{d}^{(+)} + \mathbf{d}^{(-)}, \tag{3}$$

we have

$$\mathbf{d}^{(-)} \equiv \wp \Big(|e_+\rangle\langle g|\boldsymbol{\epsilon}_+^* + |e_-\rangle\langle g|\boldsymbol{\epsilon}_-^* \Big) \; , \tag{4}$$

where $\wp$ is the reduced matrix element of the $e \leftrightarrow g$ transition and $\boldsymbol{\epsilon}_\pm \equiv \pm\frac{1}{\sqrt{2}}(\boldsymbol{\epsilon}_x \pm i\boldsymbol{\epsilon}_y)$ are circular unit vectors, where $\boldsymbol{\epsilon}_x$ and $\boldsymbol{\epsilon}_y$ are the Cartesian unit vectors in the x and y directions, respectively.

The light field is formed by two counterpropagating, crossed linearly polarized laser beams,

$$\mathbf{E}_1(Z,t) = E_0\boldsymbol{\epsilon}_x \cos(qZ - \omega t - \varphi)$$

and

$$\mathbf{E}_2(Z,t) = E_0\boldsymbol{\epsilon}_y \cos(qZ + \omega t - \varphi),$$

respectively. Here, E_0 is the amplitude of the laser fields, $\omega = cq$ is the frequency, q is the wave number, and φ is an as yet arbitrary phase.

Decomposing the total electric field $\mathbf{E} = \mathbf{E}_1 + \mathbf{E}_2$ into its positive and negative frequency parts,

$$\mathbf{E}(Z,t) = \mathbf{E}^{(+)}(Z)e^{-i\omega t} + \mathbf{E}^{(-)}(Z)e^{i\omega t}, \tag{5}$$

we have

$$\mathbf{E}^{(+)}(Z) = \frac{1}{2}E_0 \left\{ \boldsymbol{\epsilon}_x e^{i(qZ-\varphi)} + \boldsymbol{\epsilon}_y e^{-i(qZ-\varphi)} \right\}. \tag{6}$$

Since the electric field involves linear polarization, it is useful to switch from circular orbitals $|e_\pm\rangle$ to linear orbitals,

$$|x\rangle = \frac{e^{-i\varphi}}{\sqrt{2}}\Big(|e_-\rangle - |e_+\rangle \Big) \; , \tag{7}$$

$$|y\rangle = \frac{ie^{i\varphi}}{\sqrt{2}}\Big(|e_-\rangle + |e_+\rangle \Big) \; . \tag{8}$$

Expressed in terms of linear orbitals, and choosing $\varphi = \pi/4$, the magnetic dipole operator (2) becomes

$$\hat{m}_z = -\hbar g_J \mu_B \Big(|e_y\rangle\langle e_x| + |e_x\rangle\langle e_y| \Big) \; . \tag{9}$$

Furthermore, the negative frequency part of the dipole transition operator (4) becomes

$$\mathbf{d}^{(-)} = -\wp \Big(|e_x\rangle\langle g|e^{i\varphi}\boldsymbol{\epsilon}_x + |e_y\rangle\langle g|e^{-i\varphi}\boldsymbol{\epsilon}_y \Big) \; . \tag{10}$$

Finally, the state vector of the atom in the position representation appears as

$$|\Psi\rangle = \sum_s \int dZ \psi_s(Z,t)|s\rangle \otimes |Z\rangle \; , \tag{11}$$

where $s = \{x,g,y\}$ labels the internal state of the atom and Z refers to the center-of-mass position.

Inserting (9) and the product of (6) and (10) into Eq. (1), dropping antiresonant contributions in a rotating-wave approximation, and going into an interaction picture with respect to the free internal dynamics of the atom, the Hamiltonian for the state vector $(\psi_x,\psi_g,\psi_y)^T$ becomes

$$\begin{aligned} H &= \frac{\hat{P}^2}{2M} + \frac{\hbar}{2}\begin{pmatrix} 0 & \Omega e^{iq\hat{Z}} & 2\omega_L \\ \Omega e^{-iq\hat{Z}} & 0 & \Omega e^{iq\hat{Z}} \\ 2\omega_L & \Omega e^{-iq\hat{Z}} & 0 \end{pmatrix} \\ &\equiv T(\hat{P}) + V(\hat{Z}) \; , \end{aligned} \tag{12}$$

where $\Omega = \wp E_0/\hbar$ is the bare Rabi frequency and $\omega_L = g_J\mu_B B_0$ denotes the Larmor frequency. Due to the representation in terms of linear atomic orbits, Larmor precession here appears in the form of a periodic population exchange between the levels $|x\rangle$ and $|y\rangle$, a process sometimes called precession of the atomic alignment [23].

B. Magneto-optical interaction

For an atom placed at any fixed position z, the interaction matrix $V(Z)$ describes the internal dynamics of the atom in which population exchange between the ground and the excited states and the precession of the alignment appear intertwined. Population exchange takes place with the Rabi frequency Ω. The precession of the alignment, which occurs with frequency $2\omega_L$, changes the probability of absorbing or emitting photons from one laser field or the other. If the frequency of the absorption and emission cycles matches the frequency of the precession of the alignment, i.e., for $\Omega = 2\omega_L$, we expect a resonance in which the atom repeats cycles of absorption from field 1 and emission into field 2 or vice versa, leading effectively to a splitting of the atomic beam. This picture is, however, an oversimplification as neither the alignment nor the Rabi oscillations evolve freely. Further insight into the internal dynamics of the atom is provided by the eigenvalues of the magneto-optical interaction.

The interaction matrix $V(Z)$ may be diagonalized by means of a similarity transformation $U(Z)$ whose rows are the eigenstates of $V(Z)$: $U(Z)^\dagger V(Z)U(Z) = \hbar D\{\lambda_j(Z)|j = 1,2,3\}$, where D is a diagonal matrix and $|j_s(Z)\rangle = U(Z)|s\rangle$ for $s = -,g,+$. To avoid confusion with the exact eigenstates of the full Hamiltonian to be considered subsequently, we refer to the $|j_s(Z)\rangle$ as dressed states of the atom. The eigenvalues of $V(Z)/\hbar$ are given by

$$\lambda_j(Z) = 2r\cos\left(\frac{\alpha(Z)}{3} + \frac{2\pi}{3}j\right), \quad j = 1,2,3\,, \tag{13}$$

where

$$r^2 = \frac{1}{3}\left({\omega_{\rm L}}^2 + \frac{\Omega^2}{2}\right), \tag{14}$$

$$\cos[\alpha(Z)] = \frac{\omega_L\Omega^2}{4r^3}\cos(2qZ)\,. \tag{15}$$

In Fig. 2 the eigenvalues λ_j are plotted as a function of position z. The bold line depicts the eigenvalue pertaining to the dressed state $|2_g(Z)\rangle$ into which the bare state $|g\rangle$ evolves if the interaction is adiabatically switched on. The shaded bands are the exact energy bands of H to be introduced below.

In a weak laser field $\Omega \ll \omega_L$, the eigenvalues show a sinusoidal spatial modulation, oscillating around their purely magnetic values $\lambda_1 = -\omega_L$, $\lambda_2 = 0$, $\lambda_3 = \omega_L$; see upper part of Fig. 2. For increasing laser field strengths, the oscillations deviate more and more from a sinusoidal characteristic. For a field strength E_0 such that the matching condition $\Omega = 2\omega_L$ is fulfilled, exact level degeneracies appear and the middle portion of the spectrum displays the triangular spatial dependency of a blazed grating; see lower part of Fig. 2. For still larger laser field strengths $\Omega \gg \omega_L$, the magnetic effects of the precession of the alignment become insignificant, and the spectrum shows a weakly modulated spatial dependence with $\lambda_{3,1} \approx \pm\Omega/2$ and $\lambda_2 \approx 0$.

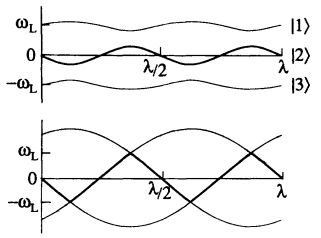

FIG. 2. The quasipotentials for the interaction eigenstates of the magneto-optical interaction as a function of position in the z direction (the thick line denotes the energy of the interaction eigenstates into which the ground state may evolve adiabatically). Upper part: $\Omega = \omega_L$. Lower part: $\Omega = 2\omega_L$. For this ratio the eigenstate $|2\rangle$ experiences a triangularly-shaped potential. The periodicity is $\lambda/2$, and the energy difference of maximum and minimum of the triangular potential is $2\hbar\omega_L$. The shaded bands are the exact energy bands which are shown in Fig. 4.

Consider now an atomic beam of ground state atoms impinging on the interaction region head-on, i.e., with $p = 0$. The atoms evolve adiabatically into the dressed state $|2_g\rangle$ and experience the potential $\lambda_2(Z)$.

For very short interaction times, the atoms have no time to move and the kinetic-energy operator may be neglected in a Raman-Nath approximation. In this approximation, the magneto-optical field appears as a thin phase grating and the outgoing beam is approximately described by a wave function $\psi_g(Z;\tau) = (2\pi)^{-1/2}\exp\{-i\lambda_2(Z)\tau\}$. The Fourier transform of that wave function gives the momentum distribution of the outgoing wave. For a laser field intensity which obeys the matching condition $\Omega = 2\omega_L$, we have $d\lambda_2/dZ \approx \pm 2\Omega q/3$, and the distribution shows two symmetrically placed peaks, separated by $\Delta p = (4/3)\hbar q\Omega\tau$. This is essentially the beam splitting effect demonstrated experimentally in Ref. [23].

For increasing interaction times, the short-time approximation becomes invalid for two reasons. First, spontaneous emission may occur which limits the applicability of a purely Hamiltonian description. We shall return to that point later and assume for the time being that interaction times are still short enough to allow spontaneous emission to be neglected. Second, the Raman-Nath approximation becomes invalid for interaction times long enough to allow the kinetic energy $(\Delta p)^2/2M$ to become of the same order as the potential energy $\hbar\Omega$. Equating $(\Delta p)^2/2M$ with $\hbar\Omega$ using $\Delta p = (4/3)\hbar q\Omega\tau$, the interaction times beyond which the Raman-Nath approximation becomes invalid is given by

$$\tau_{\rm RN} = 1/\sqrt{\omega_{\rm rec}\Omega}\,, \tag{16}$$

where $\omega_{\rm rec} = \hbar q^2/(2M)$ is the recoil frequency.

To describe situations where the interaction times exceed $\tau_{\rm RN}$, the kinetic operator must be included. It is still possible to work in the dressed-state picture described by the Hamiltonian $\tilde{H} = U(\hat{Z})^\dagger T(\hat{P})U(\hat{Z}) + \hbar D\{\lambda_j(\hat{Z})|j = 1,2,3\}$. However, because $\hat{P}$ and $U(\hat{Z})$ do not commute,

the transformed Hamiltonian $\tilde{H}$ contains off-diagonal elements which couple the dressed states. In situations where the off-diagonal elements are small compared to the energy differences $\hbar|\lambda_i - \lambda_j|$, the couplings may be neglected in an adiabatic approximation, and the motion may safely be described by three decoupled Schrödinger equations with Hamiltonians of the generic form $H_j = T(\hat{P}) + \hbar\lambda_j(\hat{Z})$.

Evidently, the conditions of the adiabatic approximation are violated at the degeneracies $\lambda_i = \lambda_j$ met under the matching condition $\Omega = 2\omega_L$ for a blazed grating. Because this configuration plays an important role for the magneto-optical beam splitting, we do not make use of the adiabatic approximation, discard the dressed-state description, and turn to the problem of an exact diagonalization of the Hamiltonian (12).

C. Magneto-optical dispersion

Motivated by the periodicity of the interaction $V(\hat{Z})$, we envision the diagonalization of H using the methods of solid-state theory. Such methods have been developed in Ref. [10] to study the related problem of the motion of a two-level atom in a standing-wave laser field.

We note first that the interaction $V(\hat{Z})$ is invariant under a translation by an optical wavelength $\lambda = 2\pi/q$. That invariance, however, covers only half of the full symmetry group of H. The interaction is also invariant under a hybrid transformation S which consists of the translation by half an optical wavelength concomitant with an inversion of the electric polarization $|g\rangle\langle x| \to -|g\rangle\langle x|$, $|g\rangle\langle y| \to -|g\rangle\langle y|$. The transformation may be represented as

$$S = \begin{pmatrix} -1 & 0 & 0 \\ 0 & 1 & 0 \\ 0 & 0 & -1 \end{pmatrix} \exp\left\{\frac{i\pi}{\hbar q}\hat{P}\right\}, \tag{17}$$

and the invariance of H under the symmetry operation S reads

$$[H, S] = 0. \tag{18}$$

Following common practice, we shall expand the eigenstates of H in the basis of eigenstates of S. The eigenstates of S are given by the electrotranslational states [10]

$$|sn\kappa\rangle = \begin{cases} |x\rangle \otimes |\kappa + (2n+1)q\rangle & \text{for } s = x \\ |g\rangle \otimes |\kappa + 2nq\rangle & \text{for } s = g \\ |y\rangle \otimes |\kappa + (2n+1)q\rangle & \text{for } s = y\ , \end{cases} \tag{19}$$

where $\langle Z|\kappa + mq\rangle = \frac{1}{\sqrt{2\pi}} e^{i(\kappa+mq)Z}$ is a plane wave with wave vector $k = \kappa + mq$, $m = 0, \pm 1, \ldots$, and κ is the Floquet exponent (crystal momentum) of the wave. The states (19) obey $S|sn\kappa\rangle = e^{i\pi\kappa/q}|sn\kappa\rangle$, i.e., $e^{i\pi\kappa/q}$ are the eigenvalues of S, and from (18) it follows that κ is a constant of motion. Restricting the values of κ to the first Brillouin zone $-q \le \kappa < q$, the set of electrotranslational states $|sn\kappa\rangle$ is orthogonal,

$$\langle sn\kappa|s'n'\kappa'\rangle = \delta_{ss'}\delta_{nn'}\delta(\kappa - \kappa')\ , \tag{20}$$

and complete,

$$1 = \sum_s \sum_n \int_{-q}^{q} d\kappa |sn\kappa\rangle\langle sn\kappa|\ . \tag{21}$$

The crystal momentum κ being conserved, every eigenstate of H may be expanded in a Fourier series for fixed κ,

$$|\phi\rangle = \sum_{sn} C_{sn}|sn\kappa\rangle\ . \tag{22}$$

In terms of the expansion coefficients C_{sn}, the stationary Schrödinger equation becomes

$$EC_{xn} = T_{2n+1}C_{xn} + \frac{\Omega}{2}C_{gn} + \omega_L C_{yn}, \tag{23}$$

$$EC_{gn} = T_{2n}C_{gn} + \frac{\Omega}{2}\left(C_{xn} + C_{yn-1}\right), \tag{24}$$

$$EC_{yn} = T_{2n+1}C_{yn} + \frac{\Omega}{2}C_{gn+1} + \omega_L C_{xn}\ , \tag{25}$$

where recoil units have been used, i.e., $E/\hbar\omega_{\rm rec} \to E$, $\Omega/\omega_{\rm rec} \to \Omega$, $\omega_L/\omega_{\rm rec} \to \omega_L$, $\kappa/q \to \kappa$, and $T_m = (\kappa + m)^2$, with $m = 0, \pm 1, \ldots$ is the kinetic energy in recoil units.

With some relabeling, the above set of equations may be brought into the form of a tridiagonal recurrence relation. The solutions of that recurrence relation are most easily obtained by means of a continued fraction method or by a suitably truncated matrix diagonalization.

For a given κ, the set of equations has infinitely many solutions E_ν, $\{C_{sn\nu}\ |s = x, g, y;\ n = 0, \pm 1, \ldots\}$, which are enumerated by a band index $\nu = 0, 1, 2, \ldots$. For a given band index ν, the energy $E_\nu(\kappa)$ and coefficients $C_{sn\nu}(\kappa)$ vary continuously as κ varies in the Brillouin zone.

The energy branches $E_\nu(\kappa)$ are shown in Fig. 3 for the freely moving atoms with only the magnetic field present, and in Fig. 4 with the laser field switched on. The parameters have been chosen for illustrative purposes; their values are $\omega_L = \omega_{\rm rec}$ (Fig. 3) and $\Omega = 2\omega_L = 2\omega_{\rm rec}$ (Fig. 4).

The magnetic interaction being spatially homogeneous, the energy branches shown in Fig. 3 are essentially the kinetic energies of a free atom, shifted by an amount $\pm\hbar\omega_L$ due to the Zeeman splitting of the excited state. In this figure, three families of energy branches may be identified which correspond to the three atomic levels under consideration. The energy branches intersect at various positions in the Brillouin zone. With the light field turned on, the intersections disappear and are replaced by anticrossings; see Fig. 4. This leads to the appearance of a band structure which is also shown in Fig. 2. Notice the narrowing of the second band as compared with the lowest lying band. The lowest lying band is related to the quasifree motion in the rather flat bottom part of the quasipotential, while the second band is related to the motion in the bottom of the triangular section of the quasipotentials. One must keep in mind, however, that

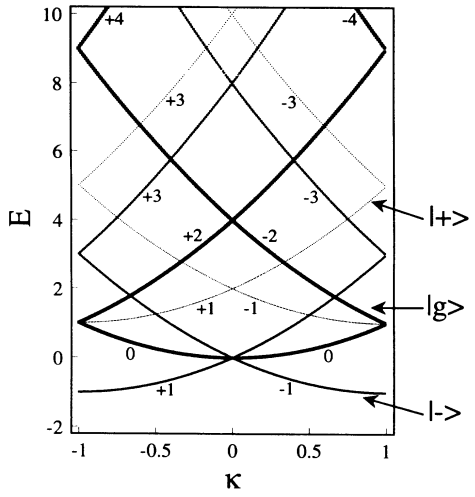

FIG. 3. The dispersion relation for a free atom in the presence of a magnetic field, $\omega_L = \omega_{\rm rec}$. The initial momentum κ is given in units of the photon momentum q, the energy in units of $\hbar\omega_{\rm rec}$. The branches with indices $m = 0, \pm 2, \pm 4, \ldots$ and $m = \pm 1, \pm 3, \ldots$ refer to the states $|g\rangle$ and $|\pm\rangle$, respectively. The energies of $|\pm\rangle$ are shifted due to the magnetic field by $\pm\hbar\omega_L$.

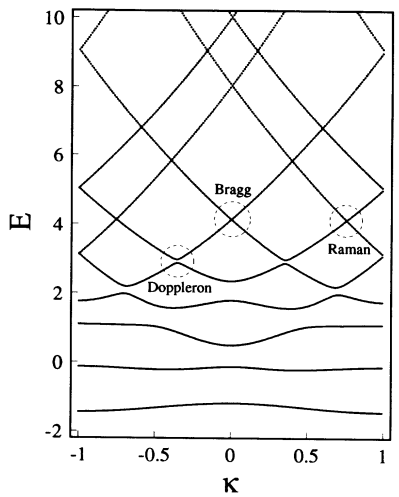

FIG. 4. The dispersion relation for an atom in the magneto-optical potential, $\Omega = 2\omega_L = 2\omega_{\rm rec}$. The intersections of the free dispersion relation become avoided crossings, leading to nearly flat energy bands for low energies. There exist three different resonances at the avoided intersections: Bragg resonance (between branches of the same family), doppleron resonance (between $|g\rangle, |+\rangle$ and between $|g\rangle, |-\rangle$), and a Raman-type resonance (between $|+\rangle, |-\rangle$).

the energy bands are not the energy bands of the quasipotentials in the adiabatic approximation, but rather of the full Hamiltonian (12).

At the anticrossings in Fig. 4, the energies nearly touch, leading to two-beam resonances (Pendellösung) in atomic beam diffraction. Three kinds of resonances may be identified. Bragg resonances involving branches of the same electronic states, velocity-tuned (doppleron) resonances involving branches of different electronic states, and a new, Raman-type class of resonances, involving branches of different Zeeman sublevels. Bragg resonances and doppleron resonances have previously been identified for a two-level atom moving in a standing-wave laser field [10]. The Raman-type resonances are identified here.

Characteristic for Bragg resonances is their position in the Brillouin zone, which is either at the center $\kappa = 0$ or at the boundaries $\kappa = \pm q$. Doppleron resonances and Raman resonances, in contrast, may appear for any value κ, the concrete value being given by the value of the Larmor frequency which here serves as an effective detuning between the laser frequency and the Bohr transition frequency. Thus, for a prescribed value ω_L, these resonances are encountered only for certain values of the atomic velocity (velocity-tuned resonances).

D. Time evolution

The set of eigenstates constructed in the previous section,

$$|\phi_\nu(\kappa)\rangle = \sum_{sn} C_{sn\nu}(\kappa)|sn\kappa\rangle \ , \tag{26}$$

is orthonormal,

$$\langle\phi_\nu(\kappa)|\phi_\mu(\kappa')\rangle = \delta_{\mu\nu}\delta(\kappa - \kappa') \ , \tag{27}$$

and complete,

$$1 = \sum_\nu \int_{-q}^{q} d\kappa |\phi_\nu(\kappa)\rangle\langle\phi_\nu(\kappa)| \ . \tag{28}$$

For the expansion coefficients, these identities imply, respectively,

$$\sum_{sn} C^*_{sn\nu} C_{sn\mu} = \delta_{\mu\nu} \ , \tag{29}$$

$$\sum_{\nu} C_{sn\nu} C^*_{s'n'\nu} = \delta_{ss'}\delta_{nn'} \ . \tag{30}$$

With the coefficients $C_{sn\nu}(\kappa)$ and energies $E_\nu(\kappa)$ numerically evaluated, the time evolution of any initial state

$$|\psi(t_0)\rangle = \int_{-q}^{q} d\kappa \sum_{sn} \beta_{sn}(t_0;\kappa)|sn\kappa\rangle \tag{31}$$

is easily obtained. We have explicitly

$$|\psi(t)\rangle = \int_{-q}^{q} d\kappa \sum_{sn} \left[\sum_{s'n'\nu} \beta_{s'n'}(t_0;\kappa) C_{s'n'\nu}(\kappa)^* C_{sn\nu}(\kappa) e^{-iE_\nu(\kappa)t} \right] |sn\kappa\rangle, \tag{32}$$

where the term in the square brackets represents $\beta_{sn}(t;\kappa)$. The coefficients $\beta_{sn}(\kappa)$ are in a simple way related to the momentum distribution of the state at time t. For example, $|\beta_{gn}(t;\kappa)|^2$ is the probability of finding the atoms at time t in the ground state, propagating with momentum $\hbar\kappa + 2n\hbar q$.

For the class of atoms impinging in the ground state with sharp momentum $p_0 = \hbar(\kappa_0 + 2n_0 q)$ (plane wave), we have $\beta_{sn}(t_0;\kappa) = \delta_{sg}\delta_{nn_0}\delta(\kappa - \kappa_0)$ and the expression for the state vector (32) reduces to a discrete sum. It is to be noted, however, that the above procedure may be applied for any arbitrary initial state, and, moreover, may be used for any arbitrary representation, including the position representation or the Wigner representation. The only operation required for the latter representation are suitable Fourier transforms of the density operator $|\psi(t)\rangle\langle\psi(t)|$, a numerical task which is accomplished most easily by fast Fourier transform techniques.

In the procedure described so far it was assumed that Ω is time independent. In general, however, the atoms experience different field strengths while traversing the interaction region as a result of the transverse profile of the laser beam. This effect is easily accounted for by a replacement $\Omega \to f(t)\Omega$, where $f(t)$ is a suitable envelope function modeling the transverse laser profile. In a numerical implementation, time is discretized such that $f(t_{i+1})$ differs only little from $f(t_i)$, and $H(t)$ is diagonalized at each time step t_i. The propagation of the initial state $|\psi(t_0)\rangle$ is then obtained from a sequence of propagations $|\psi(t_i)\rangle \to |\psi(t_{i+1})\rangle$ using $H(t_i)$ as an effective generator.

III. RESULTS

In this section we present the results of the numerical simulations of the diffraction of atoms from the magneto-optical configuration (MOD) for a variety of initial states and laser profiles. We also contrast the MOD with the diffraction of two-level atoms from a standing-wave laser field (SWD). The latter situation is described by a Hamiltonian

$$H_{\mathrm{SWD}} = \frac{\hat{P}^2}{2M} - \hbar \begin{pmatrix} \delta/2 & \Omega\cos(qZ) \\ \Omega\cos(qZ) & -\delta/2 \end{pmatrix}, \quad (33)$$

where δ is the detuning between the laser frequency and the atomic transition frequency, and Ω denotes the bare Rabi frequency of the atom-laser interaction.

The MOD results are depicted in Fig. 5, and the SWD results are depicted in Fig. 6. The figures show density plots of the momentum distribution of the outgoing atoms for incoming atoms in the electronic ground state moving with zero transverse momentum. The horizontal axis measures the momenta of the outgoing atoms in units of $\hbar q$; the vertical axis measures the effective interaction time τ in units of $\omega_{\mathrm{rec}}^{-1}$. Note that the figures do not show the time evolution during the interaction, but rather the momentum distribution after the atoms have left the interaction region. The interaction parameters are $\Omega = 160\omega_{\mathrm{rec}}$ in both cases, with matched Larmor frequency $\omega_L = \Omega/2$ for the MOD and $\delta = 0.1\Omega$ for the SWD.

Two different envelope functions $f(t)$ are used to model

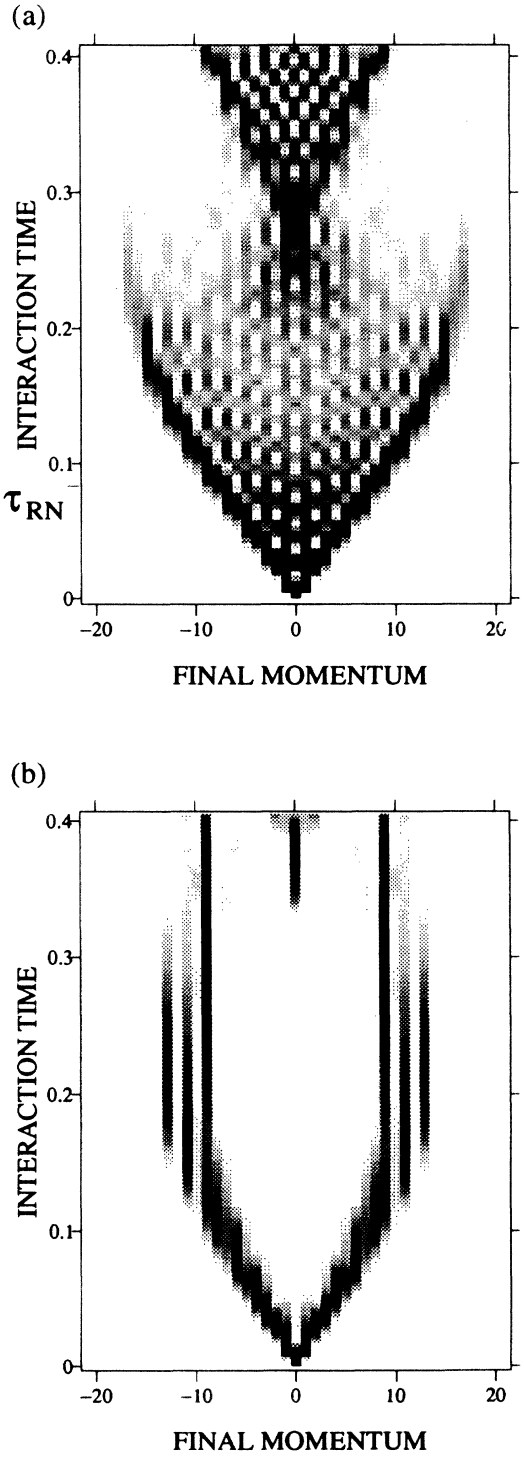

FIG. 5. Final momentum distribution for MOD (in units of $\hbar q$) as a function of interaction time (in units of $1/\omega_{\mathrm{rec}}$) for $\Omega = 2\omega_L = 160\omega_{\mathrm{rec}}$. The incoming atoms are in the ground state with zero momentum. (a) With a steplike envelope function. (b) With a Gaussian envelope function.

the possible laser profiles. Underlying in Figs. 5(a) and 6(a) is a simple step function

$$f(t) = \Theta(t - t_0) - \Theta(t - t_0 + \tau) \tag{34}$$

of duration τ. Underlying Figs. 5(b) and 6(b) is a Gaussian function

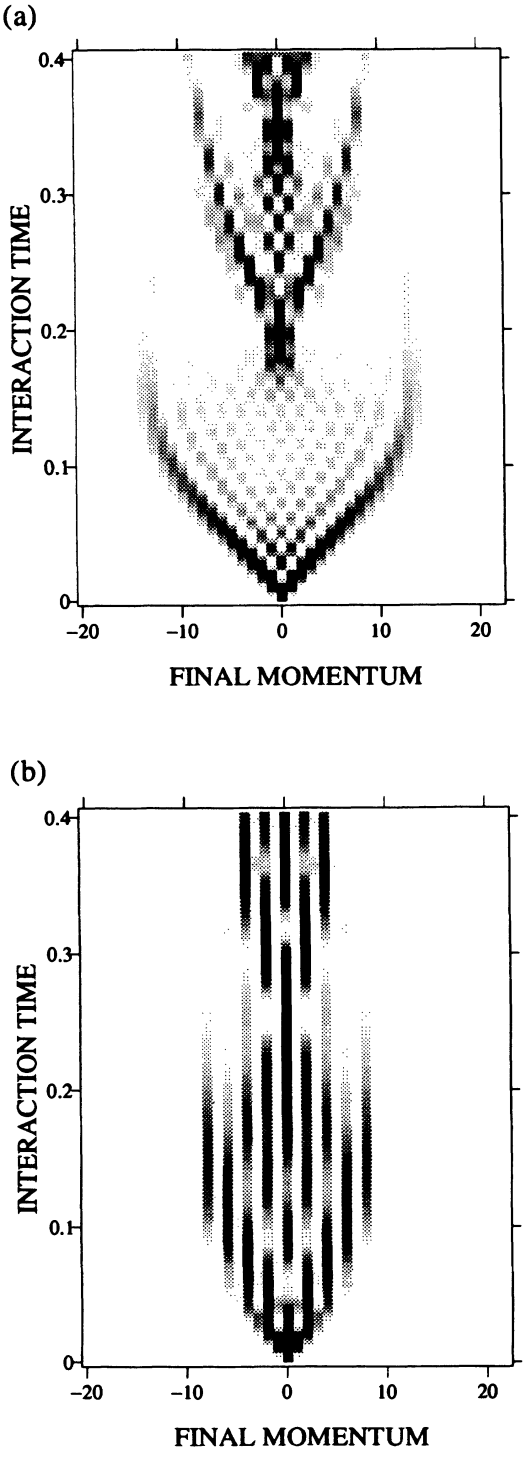

FIG. 6. Final momentum distribution for SWD with $\Omega = 160\omega_{\rm rec}$ and $\delta = 0.1\Omega$. (a) With a steplike envelope function. (b) With a Gaussian envelope function.

$$f(t) = \exp\left\{-\frac{(t - t_0)^2}{(\tau/2)^2}\right\} \tag{35}$$

of $1/e$ width τ. The steplike variation of the envelope function (34) implies nonadiabatic transitions at the entrance and at the exit of the interaction region. For the Gaussian profile, on the other hand, long interaction times imply a smooth switch-on–switch-off characteristic, which in turn implies an adiabatic evolution of the state vector while the atom enters and leaves the interaction region. Because of the nonadiabatic transitions which occur for the step function, the momentum distribution depicted in Fig. 5(a) is more uniformly spread out than in Fig. 5(b), where a clear two-beam splitting is observed.

A. Time regimes

Figures 5 and 6 show the momentum fan of the outgoing atoms as it unfolds with increasing interaction time. Clearly visible in the figures are two regimes: linear growth of the momentum spread for short interaction times and a saturation of the maximal momentum spread for longer interaction times, where also collapses and revivals occur.

1. Raman-Nath regime

Linear growth of the momentum spread is characteristic for interaction times in the Raman-Nath regime. In this regime, effects of the motion of the atoms are negligible and the interaction region acts like a pure phase grating; see the discussion in Sec. II B. Of the four situations depicted in Figs. 5 and 6, the MOD with a Gaussian laser envelope shows the cleanest two-beam splitting. This is in accordance with the nearly constant slopes of the triangular portion of the MOD quasipotentials (see Fig. 2). In the case of SWD, the sinusoidal quasipotentials have significant curvature, which is responsible for the population of intermediate momentum states observed in Fig. 6(b).

We may also compare our results to the ones reported by Adams *et al.* (Ref. [24], Sec. IV) on the occurrence of nonadiabatic transitions, which were obtained in the Raman-Nath approximation. For our calculations we used a typical maximum Rabi frequency of $\Omega = 5700\omega_{\rm rec}$ and, in analogy to [24], a Gaussian laser profile $f(t)$ with $\int dt\Omega f(t) = 20\pi$. The corresponding interaction time was about half the Raman-Nath time $\tau_{\rm RN} = 1/\sqrt{\omega_{\rm rec}\Omega}$. Our exact calculations show good agreement with their results. The momentum distribution of atoms emerging in the excited state was qualitatively the same as given in [24], Fig. 10, and the probability for nonadiabatic transitions was found to be 8%, compared to 6% in [24].

2. Collapse and revival

Characteristic for the variation of the momentum distribution with increasing interaction times beyond the

Raman-Nath regime is a sequence of collapses and revivals of the short-time pattern. The first revival is most clearly visible for the MOD with a rectangular laser profile. The revival time is essentially given by the maximum half-period of oscillations in the triangular-shaped portion of the MOD quasipotential. For the parameters underlying Fig. 2, this estimate gives $\tau_{\text{rev}} \approx 0.25$, in accordance with the value which may be read off from Fig. 5(a).

In fact, the saturation of the momentum spread and the sequence of collapse and revivals may be illustrated by a simple model of classical particles moving in the quasipotential of the atom-light interaction; see Fig. 7. The classical analog of incoming atoms with zero transverse momentum is given by a spatially uniform distribution of point particles with zero velocity. Placed in the potential region, these particles start to fall, thereby picking up momentum, the distribution of which is depicted in the density plots in Fig. 7. For the triangular potential mimicking the MOD, the momentum transfer is clearly two peaked. In this case the particles fall down the two sides of the potential. Since the slope of that potential is piecewise constant, all particles pick up the same momentum in a given time interval, leading to the two-peaked momentum distribution. For the sinusoidal potential mimicking SWD, on the other hand, the curvature of the potential implies that different particles pick up different momenta for a given time interval. Correspondingly, the momentum distribution unfolds more diffusely than for MOD. In the course of time, the particles move eventually into a region of opposite slope, and for even longer interaction times oscillations occur, the period of which is essentially given by the initial position of an individual particle relative to the minima of the potential. The first revival time at which the zero-momentum state is repopulated is given by half the maximum oscillation period. The quadratic behavior near the minima of the sinusoidal potential gives every particle in that region the same oscillation frequency. Accordingly, the revival is more pronounced for SWD than for MOD, where each particle has its own oscillation period.

Although the global features of the dependence of the momentum distribution on the interaction time can be understood in purely classical terms, important features like the exclusive population of discrete momentum states and the washout of the revivals can only be understood in wave mechanical terms. This is particularly true whenever the internal states of the atoms play an important role, for example, in the population trapping discussed in the next section.

3. *Population trapping*

An interesting effect occurs for the MOD with a Gaussian laser profile. For intermediate interaction times $\tau_{\text{RN}} < \tau < \tau_{\text{rev}}$, nearly 40% of the population of the outgoing atoms are accumulated in the ninth diffraction order, corresponding to atoms in the excited Zeeman sublevel $|-\rangle$ traveling with transverse momentum $\pm 9\hbar q$. The accumulation is relatively insensitive to variations in the interaction time, yielding a very clean and robust beam

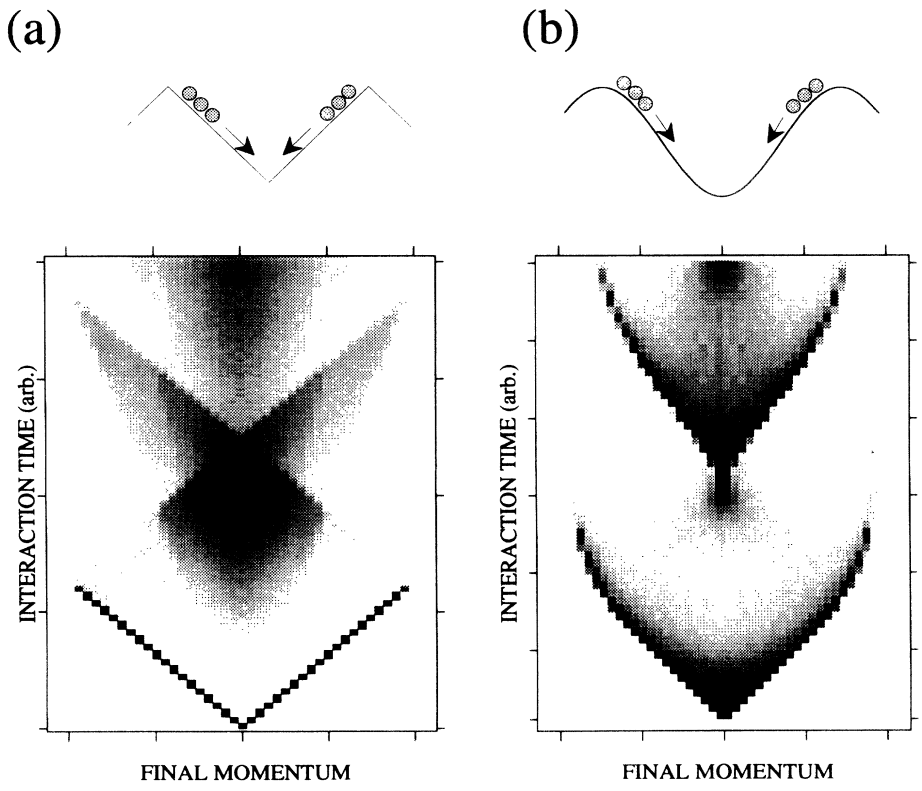

FIG. 7. A classical analog for atomic motion. Noninteracting particles with initial zero momentum move in a potential. The classical momentum distribution as a function of time is shown (a) for a triangular potential mimicking MOD and (b) for a sinusoidal potential mimicking SWD.

splitting. This population trapping can be explained as follows: For matched fields $\Omega = 2\omega_L$, the degeneracies allow transitions from state $|2\rangle$ to the energetically more favorable state $|3\rangle$. For a Gaussian envelope function, the matching condition is fulfilled only at a certain time of the interaction [$f(t) = 1$]. At other times the energy levels are well separated [Fig. 2(a)], frustrating transitions between the states. Thus, as the magneto-optical potential is switched on, the initial ground state evolves adiabatically into the state $|2\rangle$. As soon as the fields are matched, transitions occur to the state $|3\rangle$. As the potential is switched off, the degeneracies disappear. The atoms are now trapped in the state $|3\rangle$, which then evolves adiabatically into the free state $|-\rangle$.

In practice, excited atoms are experimentally unfavorable because of possible spontaneous emission which may occur on the way to the detector. To cope with this calamity, two possibilities appear at hand. The first possibility would be to use atoms with a $\wedge$ configuration of electronic states rather than the $\vee$ configuration. In this case, atoms which are initially excited would be split in the manner shown in Fig. 5(b) and the atoms would emerge in the ground state. The second possibility would be to keep the $\vee$ configuration, but to apply a π pulse just behind the interaction region. This would bring all atoms from the excited state coherently back into the ground state, thereby avoiding spontaneous emission in the following free flight to the detector.

4. Bragg regime

For Gaussian interaction times exceeding the recoil time ω_{rec}^{-1}, the evolution of the atomic state vector is adiabatic not only with respect to the internal state of the atom but also with respect to the translational motion. In the language of the band theory, the zero-momentum state is energetically sufficiently far off other states (more than $\hbar\omega_{\text{rec}}$), such that the slow variation of the Gaussian envelope does not admit any population of outgoing states other than the zero-momentum state. Accordingly, the incoming atom leaves the interaction region with most of its population in the same momentum state as it had initially; see Fig. 8(a). On the other hand, for incoming atoms which fulfill a Bragg condition, even the slowest switching on of the interaction leads to a population of two diffraction orders because the energies of the free atom are degenerate. This effect is illustrated in Fig. 8(b), which depicts the unfolding of the momentum fan for incoming atoms moving with transverse momentum $2\hbar q$. As this momentum state is energetically degenerate with the momentum state $-2\hbar q$, strong coupling between these two states appears inside the interaction region, leading to the Pendellösung behavior of the outgoing atoms as a function of the interaction time. The frequency of these oscillations is essentially given by the energetic level splitting at the avoided crossing located at the Bragg resonance.

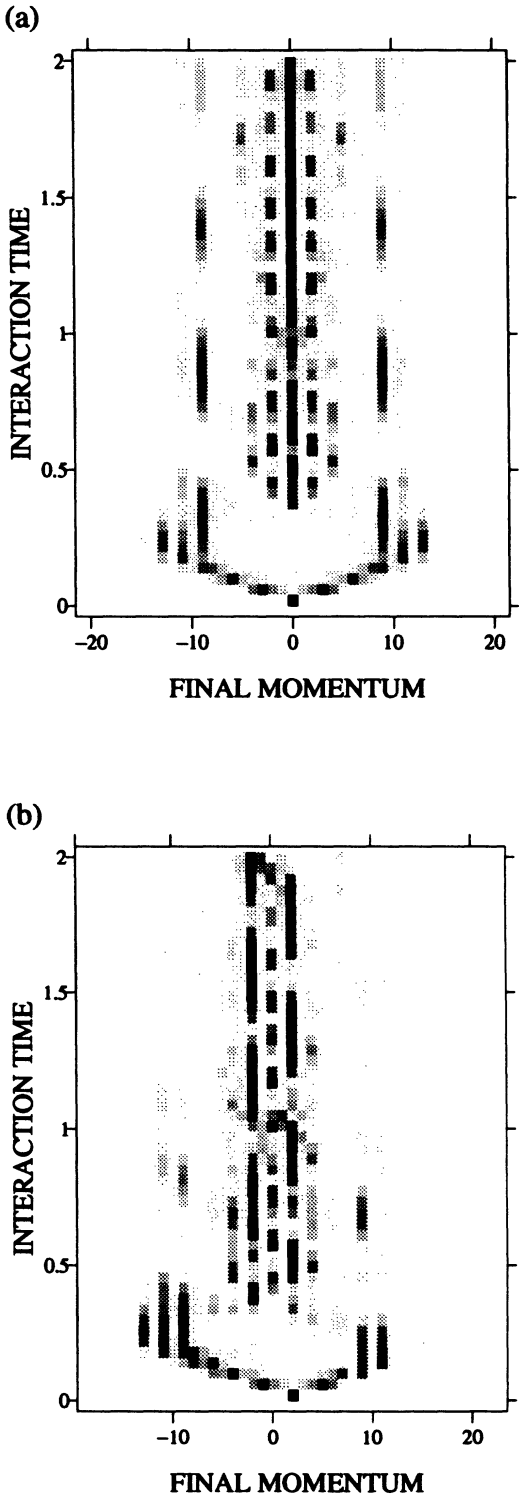

FIG. 8. Momentum transfer for MOD with a Gaussian envelope function and $\Omega = 2\omega_L = 160\omega_{\text{rec}}$ for long interaction times. The atoms are initially in the ground state. (a) Initial momentum zero. In the adiabatic regime $\tau > 1/\omega_{\text{rec}}$ the atoms leave the interaction region with zero momentum. (b) Initial momentum $2\hbar q$. For $\tau > 1/\omega_{\text{rec}}$ the final momentum distribution oscillates between $\pm 2\hbar q$.

B. Postinteraction spontaneous emission

While spontaneous emission is unlikely to occur during the interaction, this is not the case for the free flight to the detector. The reason is that the distance between the interaction region and the detection screen should be as large as possible to increase the accuracy of the resolution of the diffraction pattern. This makes spontaneous emission of atoms leaving the interaction region in an excited state almost unavoidable. To illustrate the impact of a possible single spontaneous emission act following the interaction, we simulated the magneto-optical diffraction of Ca, with the laser field tuned on resonance with the intercombination line $4\,^1S_0 - 4\,^3P_1$. For this line $\Gamma = 2.5$ kHz (radiative lifetime 0.4 ms) and $\omega_{\rm rec}/2\pi = 11.5$ kHz. For our simulations we chose $\Omega = 2\omega_L = 4600\Gamma$, which corresponds to a Raman-Nath time $\tau_{\rm RN} \approx 1$ μs, a Gaussian envelope to model the profile of the laser beam, and we also included effects of a finite detector resolution of $0.4\hbar q$. The incoming atoms are assumed to be in the ground state, traveling with zero transverse momentum.

The results of our simulations are depicted in Fig. 9. In Fig. 9(a), we show the momentum distribution of the outgoing atoms for an interaction time which lies between the Raman-Nath time and the first revival time (the dotted lines show the results without the impact of spontaneous emission). The two-beam splitting is still well visible, although the two outgoing beams appear significantly broadened as a result of the spontaneous emission. In Fig. 9(b), the interaction time is of the order of the first revival time. Here, the recurrence of the central peak is clearly visible. In contrast to the outermost peaks, which are broadened by spontaneous emission, the broadening of the central peak is entirely due to the finite resolution of the detector. Broadening by spontaneous emission does not occur because the central peak corresponds to atoms which leave the interaction region in the ground state.

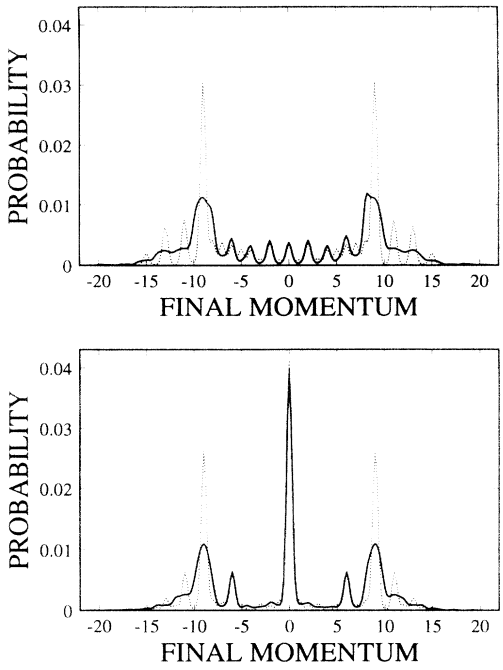

FIG. 9. Momentum distribution for Ca with $\Omega = 2\omega_L = 4600\Gamma$, where $\Gamma = 2.5$ kHz. Spontaneous emission is included by a quantum Monte Carlo simulation (the dashed lines denote the results without the impact of spontaneous emission). The incoming atoms are in the ground state with $\kappa = 0$, the detector resolution is modeled to be $0.4\hbar q$, where $\hbar q$ is the photon momentum. (a) $\tau = 0.327/\omega_{\rm rec} = 4.5$ μs, (b) $\tau = 0.380/\omega_{\rm rec} = 5.3$ μs.

IV. SUMMARY

A thorough study of the motion of three-level atoms in a magneto-optical field has been presented. The considerations are based on an exact diagonalization of the underlying Hamiltonian including the kinetic-energy operator of the atoms. The diagonalization has been accomplished in a band-theoretical framework.

The band theory allows one to identify, beside the well-known Bragg and doppleron resonances, a class of velocity-tuned resonances, where the magnetic state of the atom changes concomitant with a momentum transfer of an even number of photon recoils.

For the diffraction of atoms, three time scales have been identified. For interaction times shorter than the Raman-Nath time $\tau_{\rm RN}$, the spread of the momentum distribution increases linearly with increasing interaction time. For interaction times of the order of $\tau_{\rm RN}$, saturation of the momentum spread appears as a result of the phase mismatch reflecting the physical motion of the particles. For interaction times beyond $\tau_{\rm RN}$, the momentum distribution shows features of collapse and revival reflecting the periodic motion of the atoms in the interaction region.

The theory has been presented in such a way that it is easily adaptable for other configurations of the atom-radiation interaction as well as for other representations, such as the Wigner representation.

ACKNOWLEDGMENTS

Fruitful discussions with C. S. Adams and T. Pfau are gratefully acknowledged. M.W. acknowledges support by the Deutsche Forschungsgemeinschaft and hospitality in the group of Professor J. Mlynek.

[1] P. E. Moskowitz, P. L. Gould, S. R. Atlas, and D. E. Pritchard, Phys. Rev. Lett. **51**, 370 (1983).
[2] P. L. Gould, G. A. Ruff, and D. E. Pritchard, Phys. Rev. Lett. **56**, 827 (1986).
[3] P. J. Martin *et al.*, Phys. Rev. A **36**, 2495 (1987).
[4] P. J. Martin, B. G. Oldaker, A. H. Miklich, and D. E. Pritchard, Phys. Rev. Lett. **60**, 515 (1988).
[5] J. J. McClelland, R. E. Scholten, E. C. Palm, and R. J. Celotta, Science **262**, 877 (1993).
[6] A. Hemmerich and T. W. Hänsch, Phys. Rev. Lett. **68**,

1492 (1992).
[7] P. Verkerk, B. Lounis, and C. Salomon, Phys. Rev. Lett. **68**, 3861 (1992).
[8] A. Hemmerich and T. W. Hänsch, Phys. Rev. Lett. **70**, 410 (1993).
[9] G. Grynberg *et al.*, Phys. Rev. Lett. **70**, 2249 (1993).
[10] M. Wilkens, E. Schumacher, and P. Meystre, Phys. Rev. A **44**, 3130 (1991).
[11] Y. Castin and J. Dalibard, Europhys. Lett. **14**, 761 (1991).
[12] E. Schumacher, M. Wilkens, P. Meystre, and S. Glasgow, Appl. Phys. B **54**, 451 (1992).
[13] B. Lounis *et al.*, Europhys. Lett. **21**, 13 (1993).
[14] P. Marte, R. Dum, R. Taieb, and P. Zoller, Phys. Rev. A **47**, 1378 (1993).
[15] M. A. M. Marte and P. Zoller, Appl. Phys. B **54**, 477 (1992).
[16] P. Storey, M. Collett, and D. Walls, Phys. Rev. Lett. **68**, 472 (1992).
[17] T. Sleator and M. Wilkens, Phys. Rev. A **48**, 3286 (1993).
[18] P. Meystre, E. Schumacher, and S. Stenholm, Opt. Commun. **73**, 443 (1989).
[19] A. M. Herkommer, V. M. Akulin, and W. P. Schleich, Phys. Rev. Lett. **69**, 3298 (1992).
[20] R. Grimm, Y. B. Ovchinnikov, A. I. Sidorov, and V. S. Letokhov, Opt. Commun. **48**, 18 (1992).
[21] R. Grimm, V. S. Letokhov, Y. B. Ovchinnikov, and A. I. Sidorov, Pis'ma Zh. Eksp. Teor. Fiz. **54**, 611 (1991) [JETP Lett. **54**, 615 (1991)].
[22] R. Grimm, V. S. Letokhov, Y. B. Ovchinnikov, and A. I. Sidorov, J. Phys. II **2**, 93 (1992).
[23] T. Pfau, C. S. Adams, and J. Mlynek, Europhys. Lett. **21**, 439 (1993).
[24] C. S. Adams, T. Pfau, C. Kurtsiefer, and J. Mlynek, Phys. Rev. A **48**, 2108 (1993).
[25] T. Pfau *et al.*, Phys. Rev. Lett. **71**, 3427 (1993).
[26] H. J. Carmichael, *An Open System Approach to Quantum Optics* (Springer, Berlin, 1993).
[27] J. Dalibard and Y. Castin, Phys. Rev. Lett. **68**, 580 (1992).
[28] K. Mølmer, Y. Castin, and J. Dalibard, J. Opt. Soc. Am. B **10**, 524 (1993).

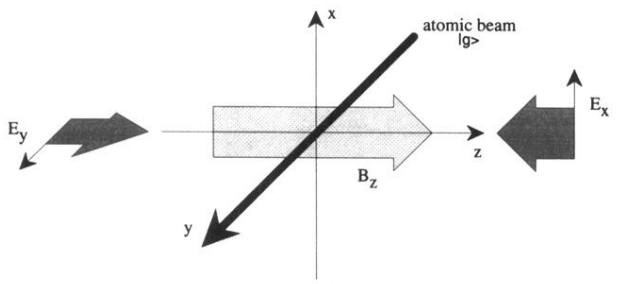

FIG. 1. The principal setup for the magneto-optical interaction.

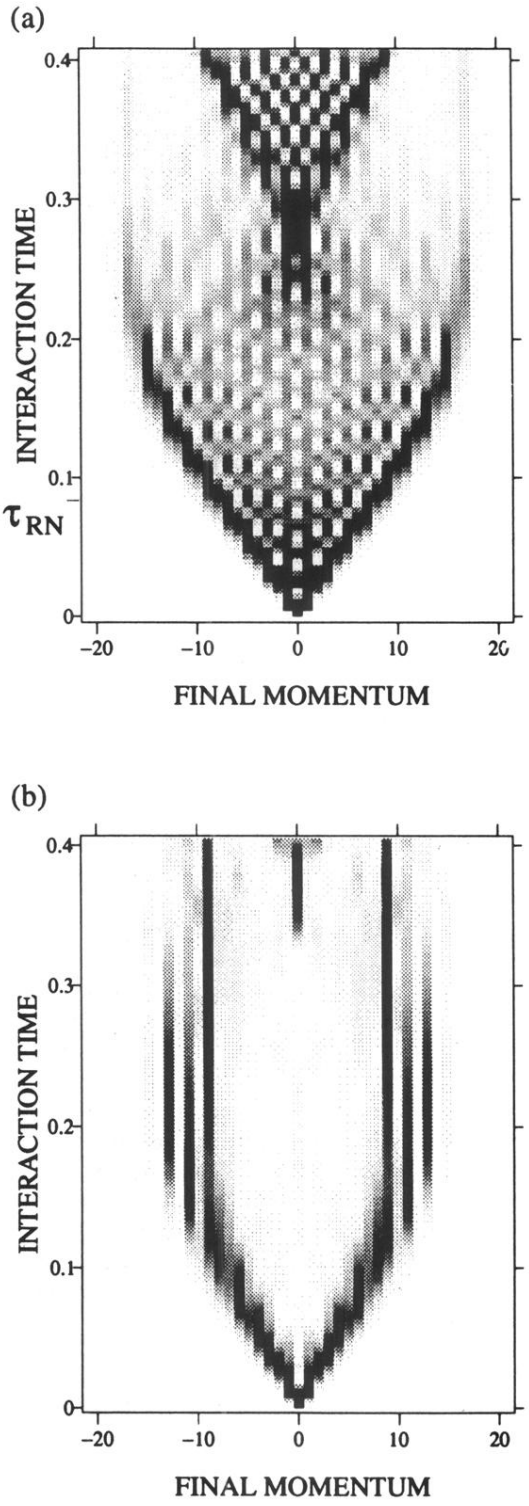

FIG. 5. Final momentum distribution for MOD (in units of $\hbar q$) as a function of interaction time (in units of $1/\omega_{\rm rec}$) for $\Omega = 2\omega_L = 160\omega_{\rm rec}$. The incoming atoms are in the ground state with zero momentum. (a) With a steplike envelope function. (b) With a Gaussian envelope function.

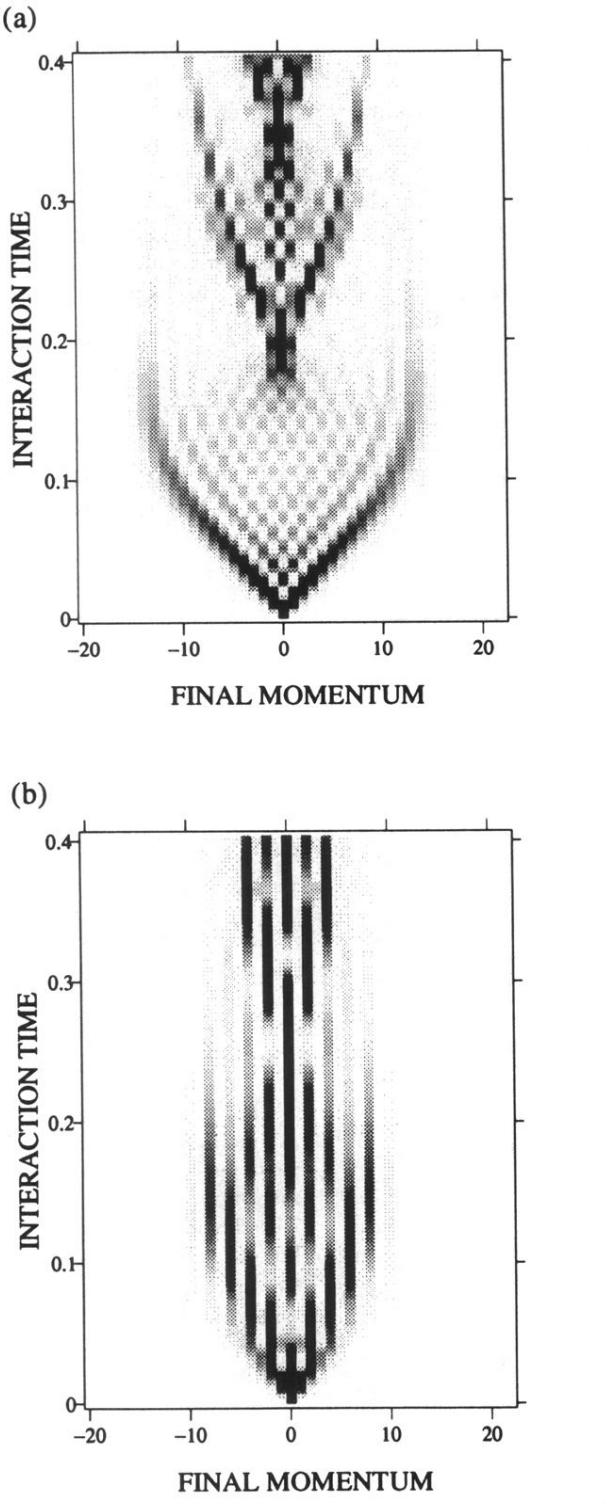

FIG. 6. Final momentum distribution for SWD with $\Omega = 160\omega_{\mathrm{rec}}$ and $\delta = 0.1\Omega$. (a) With a steplike envelope function. (b) With a Gaussian envelope function.

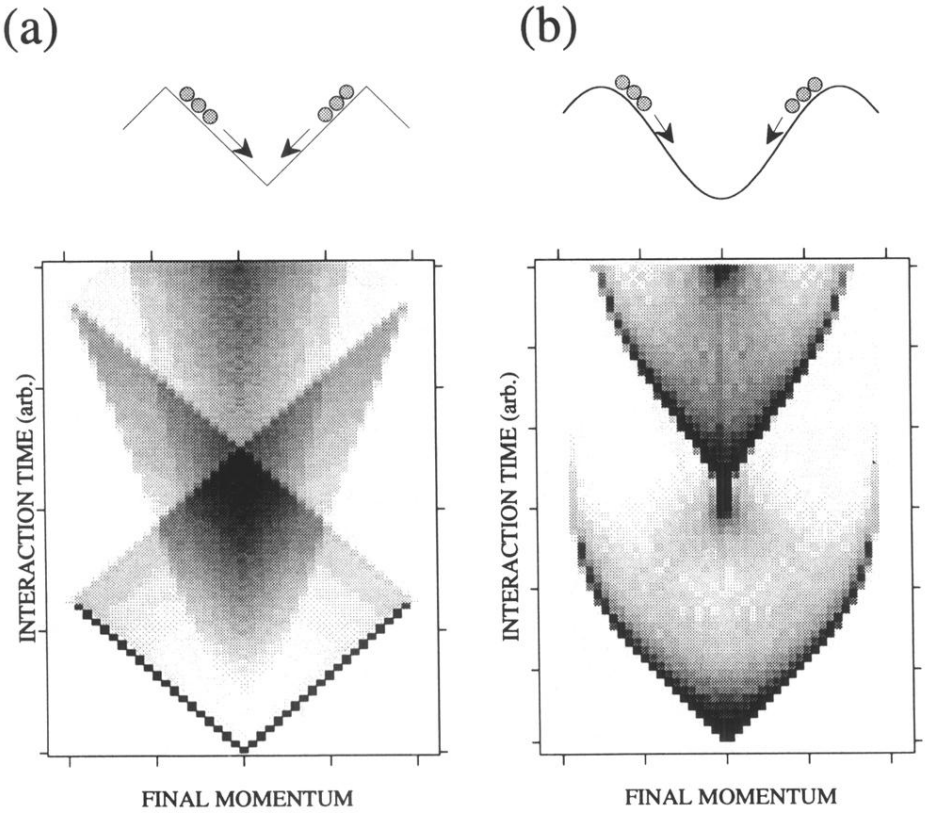

FIG. 7. A classical analog for atomic motion. Noninteracting particles with initial zero momentum move in a potential. The classical momentum distribution as a function of time is shown (a) for a triangular potential mimicking MOD and (b) for a sinusoidal potential mimicking SWD.

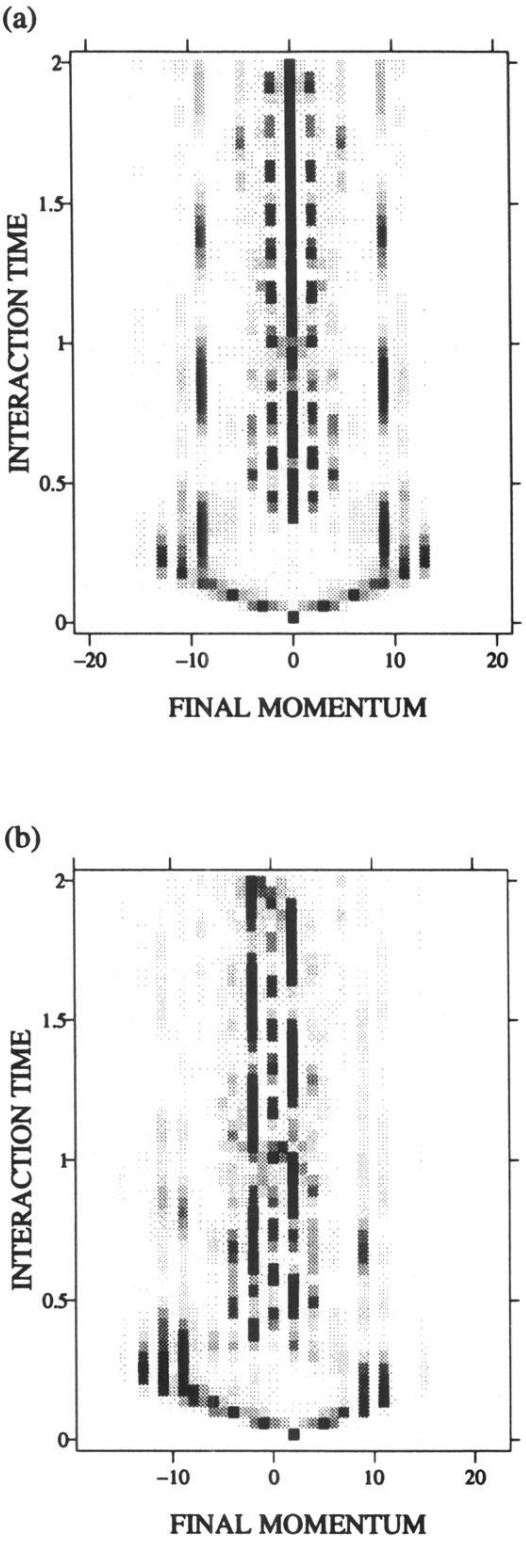

FIG. 8. Momentum transfer for MOD with a Gaussian envelope function and $\Omega = 2\omega_L = 160\omega_{\rm rec}$ for long interaction times. The atoms are initially in the ground state. (a) Initial momentum zero. In the adiabatic regime $\tau > 1/\omega_{\rm rec}$ the atoms leave the interaction region with zero momentum. (b) Initial momentum $2\hbar q$. For $\tau > 1/\omega_{\rm rec}$ the final momentum distribution oscillates between $\pm 2\hbar q$.